12-2015

Application of the aeroacoustic analogy to a shrouded, subsonic, radial fan.

Bryan Buccieri
University of Louisville

APPLICATION OF THE AEROACOUSTIC ANALOGY TO A SHROUDED,

SUBSONIC, RADIAL FAN

By
Bryan Buccieri
B.S., Rose-Hulman Institute of Technology, 2012

A Thesis
Submitted to the Faculty of the
University of Louisville
J.B. Speed School of Engineering
In Partial Fulfillment of the Requirements
For the Degree of

Master of Science in Mechanical Engineering

Department of Mechanical Engineering
University of Louisville
Louisville, KY

December 2015

APPLICATION OF THE AEROACOUSTIC ANALOGY TO A SHROUDED,

SUBSONIC, RADIAL FAN

Submitted by:

Bryan Buccieri

A Thesis Approved On

November 24th, 2015

By the Following Examination Committee:

_____

Dr. Chris Richards, Thesis Director

_____

Dr. Yongsheng Lian

_____

Dr. Eric Berson

DEDICATION

This thesis is dedicated to my mom

Nancy E. Buccieri

For her unconditional love and support

ACKNOWLEDGEMENTS

I would like to thank my advisor Dr. Richards and for his help and guidance throughout this project. My specials thanks to Scott Welham, Tim Oconnell, Chris Omalley, and Senthil Nathan for allowing me to do research and giving me their support.

ABSTRACT

APPLICATION OF THE AEROACOUSTIC ANALOGY TO A SHROUDED,

SUBSONIC, RADIAL FAN

Bryan Buccieri

November 16th, 2015

A study was conducted to investigate the predictive capability of computational aeroacoustics with respect to a shrouded, subsonic, radial fan. A three dimensional unsteady fluid dynamics simulation was conducted to produce aerodynamic data used as the acoustic source for an aeroacoustics simulation. Two acoustic models were developed: one modeling the forces on the rotating fan blades as a set of rotating dipoles located at the center of mass of each fan blade and one modeling the forces on the stationary fan shroud as a field of distributed stationary dipoles. Predicted acoustic response was compared to experimental data. The blade source model predicted overall far field sound power levels within 7 dBA and the shroud model predicted overall far field sound power levels within 14 dBA. Doubling the density of the computational fluids mesh and using a scale adaptive simulation turbulence model increased broadband noise accuracy. However, computation time doubled and the accuracy of the overall sound power level prediction improved by only 1 dBA.

TABLE OF CONTENTS

LIST OF TABLES

LIST OF FIGURES

1.   INTRODUCTION

Subsonic centrifugal fans are widely used in many industrial applications. Their purpose is to provide airflow in a system that requires a large pressure rise. The widespread use of these fans in consumer products has led to the necessity of being able to predict and reduce the noise emitted by the fan. Being able to predict tonal and broadband radiated noise is important because it will aid in the design process of fans in order to meet radiated sound regulations and consumer demands. To this end, a number of researchers have focused on predicting noise emitted from these fans.

There have been several papers published on predicting noise using computational aeroacoustics (CAA). The aeroacoustic analogy was first developed by Lighthill (1952). Lighthill derived an inhomogeneous wave equation to quantify the turbulent pressure fluctuations that generate outlet restriction noise. This analogy was enhanced by Curle (1955) to include the effects of solid surfaces on sound generation. Williams & Hawkings (1969) later improved the analogy to include the effect of moving solid surfaces on noise generation and created the Ffowcs Williams Hawkings (FW-H) aeroacoustic analogy. The FW-H aeroacoustic analogy is applicable only when the path from the source and observer is unobstructed. When there is an obstruction, such as is the case in ducted fans or fans with shrouds, the effects of propagation, diffraction, and scattering must be taken

into consideration. The Kirchhoff Formulation detailed by Lyrnintzis (2003) accounts for propagation, diffraction and scattering effects of solid boundaries such as the fan shroud.

Colonius & Lele (2004) provide a detailed review of CAA, pointing to the fact that most modern CAA methods are an application of the FW-H aeroacoustic analogy paired with a computational fluid dynamics (CFD) model. This relatively recent trend is due to the computational power now widely available, which allows for accurate computational prediction of airflow in a shrouded, subsonic, radial fan. Jeon, Baek, & Kim (2003) solved for the unsteady flow field of a shrouded, radial fan via the vortex method and then applied the FW-H aeroacoustic analogy. Jeon et al. (2003) confirmed experimentally that the aerodynamic forces in a shrouded, radial fan could be calculated numerically and used as an acoustic source for a CAA model.

There have been several recent papers that have solved for the unsteady flow field in the fan with computational fluid dynamics (CFD) that uses a turbulence model and then applies the FW-H aeroacoustic analogy to calculate the sound radiated by the a fan. Younsi, Bakir, Kouidri & Rey (2008) achieved some success in predicting the tonal component of the sound generated by a shrouded, radial fan in the free field by solving the Unsteady Reynolds Averaged Navier Stokes (URANS) equations using the k omega Shear Stress Transport (kω-SST) turbulence model summarized by Menter, Kuntz, & Langtry (2003) and applying the FW-H aeroacoustic analogy. Younsi et al. (2008) used only the fan blade surfaces as sources and ignored the fan shroud as a possible source. However, the broadband component of the noise is not captured by the model employed by Younsi et al. (2008). This is possibly due to: the use of the kω–SST turbulence model,

not accounting for diffraction, focusing and scattering effects of the fan shroud in their model, or only considering the fan blade surfaces as acoustic sources.

Mendonca, Allen, De Charentenay & Lewis (2002) found that CFD models that incorporate the large eddy simulation (LES) turbulence model are capable of producing acoustic sources that better predict broadband noise content. However, the LES turbulence model is significantly more computationally expensive than the kω–SST model. The detached eddy simulation (DES) turbulence model discussed by Mendonca et al. (2002) uses the kω–SST model near solid boundaries and transitions to the LES model away from solid boundaries. This attempts to reduce the computational effort by minimizing the number of LES calculations. Using the DES model, Tournour, Hachemi, Read, Mendonca, Barone & Durello (2003) were able to more accurately calculate the broadband noise content of a shrouded, radial fan using only the fan blade surfaces as acoustic sources. This is possibly due to the use of the DES model or that in addition, Tournour et al. (2003) account for the diffraction, focusing and scattering effects of the fan shroud in their model.

This study will compare the predicted result of a CAA model that uses the kω-SST model to a CAA model that uses the scale adaptive simulation (SAS) model discussed by Menter & Egorov (2005). The SAS model is similar to the DES model in that it transitions between the kω-SST and LES models in an attempt to improve computational efficiency. However, the SAS model uses a computational mesh size filter to determine the transition between the two models. Both models considered account for diffraction, focusing and scattering effects. This study also compares the effects of using the fan blade surfaces versus the fan shroud surfaces as acoustic source.

The shrouded, radial, subsonic fan in this study is first tested in an airflow chamber at different speeds and duct restrictions to measure various operating flow rates. These flow rates provide a metric to correlate the CFD model to the measured data. The fan is then tested in a semi-anechoic chamber were the sound pressure level (SPL) is measured with a microphone grid in order to calculate the overall far field sound power level (SWL). Computational fluid dynamics models, as described above, are used to predict the transient flow in the radial fan and shroud. The simulated transient flow data is then used in a CAA model to predict the overall far field SWL. These predictions are compared to the experimentally measured far field SWL to evaluate the accuracy of the modeling techniques. The turbulence model, CFD computational mesh density, and choice of acoustic source are compared with respect to computational cost versus prediction benefit.

2.   PROBLEM FORMULATION

The fan to be analyzed is a sub sonic radial blower with a shroud and duct with outlet restriction. The fan blades are forward curved and the diameter of the impeller is 222 mm. Figure 1 shows a detailed view of the fan rotor and fan shroud.
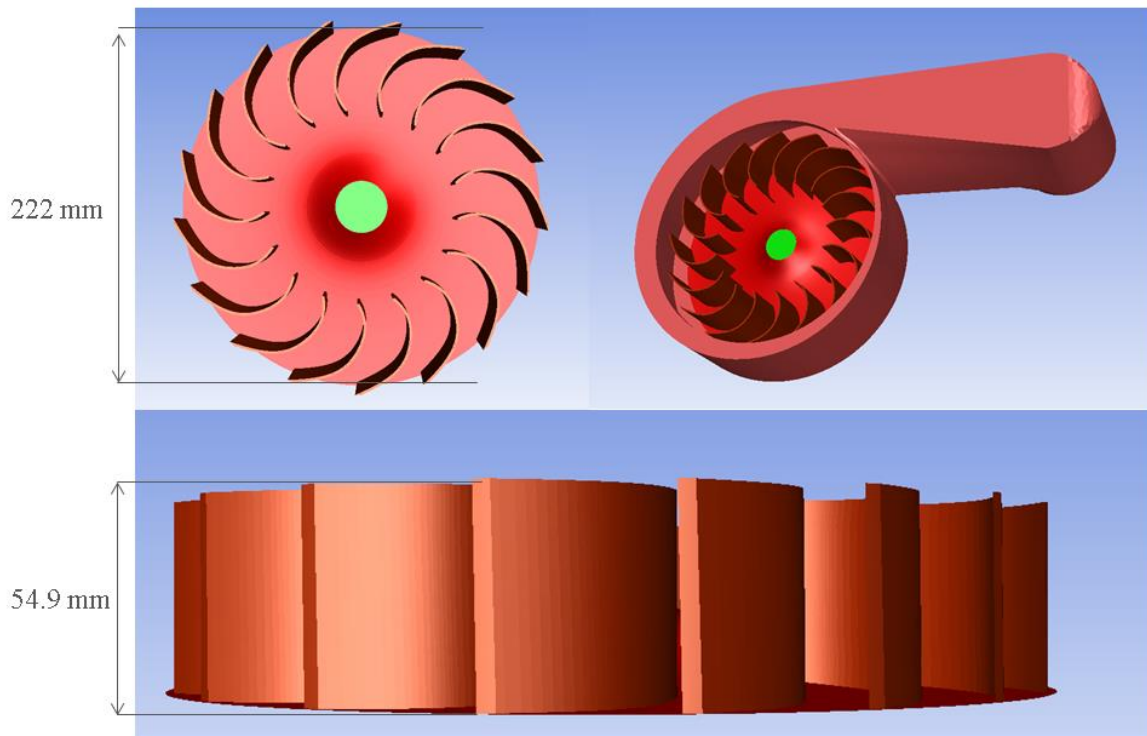
Figure 1: Dimensions of sub sonic fan analyzed.

The transient flow field is spatially discretized using two different computational mesh densities and calculated using two different turbulence models: the kω-SST and the SAS turbulence model. Assumptions made by the CFD model include incompressible, isothermal fluid, no slip boundary conditions on all walls, and negligible gravitational effects. The boundary conditions of the inlet and outlet of the fan are atmospheric

pressure. The fan blades rotate at a constant speed. The predicted flow field creates forces that are used in acoustic source models. Two separate source models are used: one uses the forces on the fan blades as acoustic sources and the other uses the forces on the fan shroud as acoustic sources. The forces on the fan blades are modeled as a series of rotating dipoles at the center of gravity of each blade. The forces on the fan shroud are modeled as a field of stationary distributed dipoles. The acoustic response is calculated from these two sources separately using the FW-H aeroacoustic analogy. The far field SWL is calculated for these two separate models using Kirchhoff's method and compared to measured results for a range of operating conditions with differing fan rotational speeds and outlet restrictions.

3.   METHOD

3.1 AERODYNAMIC METHODS

The fluid domain is spatially discretized into a computational mesh composed of tetrahedral and hexahedral cells. This computational mesh is divided into two zones: a zone surrounding the fan blades that rotate at the speed of the fan and a stationary zone comprising of the stationary shroud of the fan. The zones are coupled together with a sliding mesh interface (ANSYS 2015). To avoid errors in interpolation between the two zones, the ratio of cell sizes between the zones is kept to 1:1.

In order to solve for the time dependent flow characteristics of the radial fan, the URANS equations summarized by Date (2005) are solved using the Finite Volume Method described by Eymard, Gallouet & Herbin (1997) and a turbulence model. Two separate fluid dynamics models are constructed: One models turbulence using kω-SST and the other models turbulence using SAS. The kω-SST model is accurate and reliable for a wide range of flows and takes into consideration compressibility, low Reynolds number modifications, and adverse pressure gradients. The SAS turbulence model created by Menter & Egorov (2005), acts as a LES model where the computational mesh size is larger than turbulent eddies. The SAS acts as kω-SST in areas where the computational mesh size is smaller than turbulent eddies, typically near solid boundaries. The LES model splits up the computational grid into sub grids and calculates turbulence on these

7

sub grids. This adds to the computational cost. Therefore, the SAS model attempts to reduce this cost by only computing the LES sub grid in regions away from solid walls where the benefit to the accuracy of the aerodynamic prediction would be significant.

3.2 ACOUSTIC METHODS

The FW-H aeroacoustic analogy is used in this work (Williams & Hawkings 1969). The governing equation of this methodology is the compressible Navier-Stokes equation:

$$\frac{1}{c_0^2}\frac{\partial^2 p'}{\partial t^2} - \frac{\partial^2 p'}{\partial x_i \partial x_j} = \frac{\partial \dot{Q}}{\partial t} - \frac{\partial F_i}{\partial x_i} + \frac{\partial^2 T_{ij}}{\partial x_i \partial x_j} \tag{1}$$

where p' is the acoustic pressure, $\dot{Q}$ is the mass flow rate per unit volume of air, i represents the three Cartesian coordinates (1,2,3) j represents the spatial node, F_i is the force density acting on the fluid, T_{ij} is the Lighthill stress tensor containing momentum flux, thermal and viscous terms and c_0 is the speed of sound. Equation (1) expresses a linear wave problem. The acoustic source terms are gathered on the right hand side of the equation. The first term shows that if incompressible mass is added to the system at an unsteady rate, noise will be generated. According to Russell (1999), the resulting change in volume generates a sound that is best modeled as a monopole acoustic source. The displacement of air by the fan blades is the mechanism for this change in volume. According to Sorguven, Dogan, Bayraktar & Sanliturk (2009), if the Mach number is below 0.6, the contribution of this term is negligible. The second term shows that a spatial force gradient acting on the fluid will generate sound. Russell states that dipoles – two equivalent side-by-side monopoles acting out of phase – best model the net force on the surrounding fluid; and that, it is the net force acting on the surrounding fluid that

8

creates sound, and not the displacement of fluid. In rotating machinery such as radial fans, the forces acting on the fan casing act as distributed stationary dipoles and the forces on the rotating fan blades act as rotating dipoles at the center of gravity of each acoustically compact segment of fan blade. The last term on the right hand side of the equation shows that when time-dependent stresses, including momentum, viscosity and turbulence act on a fluid, noise will be generated. Russell states that no net force or flux acts on the fluid. However, there is a fluctuating stress on the fluid, which is best modeled as a quadrupole – two equal dipoles acting out of phase. According to Sorguven et al. (2009), if the Mach number is less than 0.8, this quadrupole source is negligible.

For the system under consideration, Mach number can be determined by first calculating the exit airspeed from the duct. The exit airspeed is calculated by dividing the measured volumetric flow rate by the exit area. Mach number is then the ratio of the exit air speed to the speed of sound. Table 1 shows the maximum Mach numbers of the three different outlet restrictions. The volumetric flow data in Table 1 was taken from the maximum measured flow rates discussed later in the results section of this paper.

Outlet Restiction Diameter (mm)	Volumetric Flow Rate (m^3/s)	Average Duct Exit Airspeed (m/s)	Mach Number
76.2	7.92E-02	17.37	5.10E-02
69.9	6.35E-02	16.56	4.87E-02
63.5	4.96E-02	15.66	4.60E-02

Table 1: Fan system maximum Mach numbers for each outlet airflow restriction.

As seen in Table 1, all of the Mach numbers are much less than the 0.6 threshold required to ignore the monopole source and the 0.8 threshold for the quadrupole source term.

Therefore, the FW-H aeroacoustic analogy simplifies to only taking into consideration the dipole sources:

$$\frac{1}{c_0^2}\frac{\partial^2 p'}{\partial t^2} - \frac{\partial^2 p'}{\partial x_i \partial x_j} = -\frac{\partial F_i}{\partial x_i} \qquad (2)$$

There are two possibilities for the dipole source term: the forces on the rotating fan blades, which act as a series of rotating dipoles; and, the forces on the interior of the shroud of the fan system, which act as a field of distributed stationary dipoles. Both sources are not considered simultaneously. Rather, two separate acoustic models are constructed: one using rotating dipoles and one using distributed stationary dipoles.

Figure 2 shows the locations of the dipole sources with respect to the geometry of the fan shroud and blades.
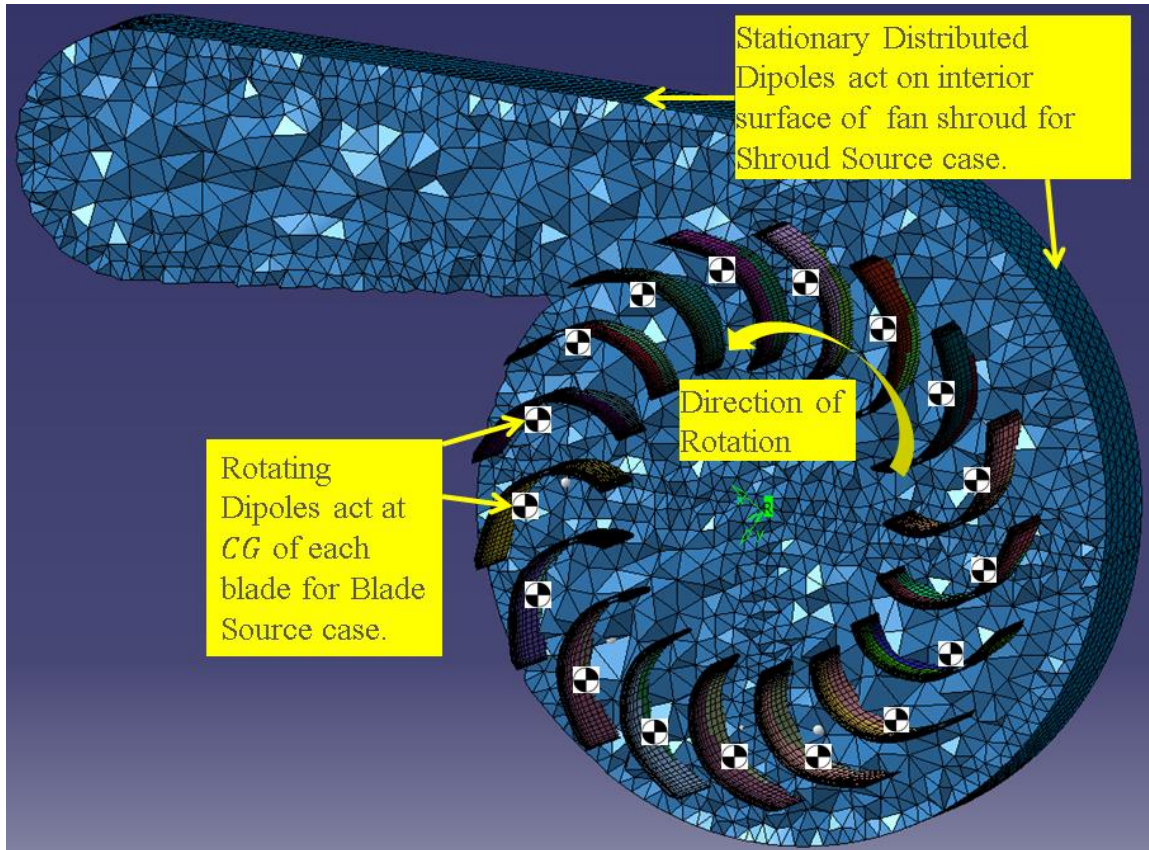
Figure 2: Acoustic source locations for rotating (Blade Source) and stationary (Shroud Source) dipoles.

The rotating dipole sources are located at the center of gravity of each acoustically compact blade segment. The stationary dipole sources are located at each spatial node on the fan shroud.

Figure 3 shows the orientation of the rotating fan blade segment with respect to the axis of rotation.
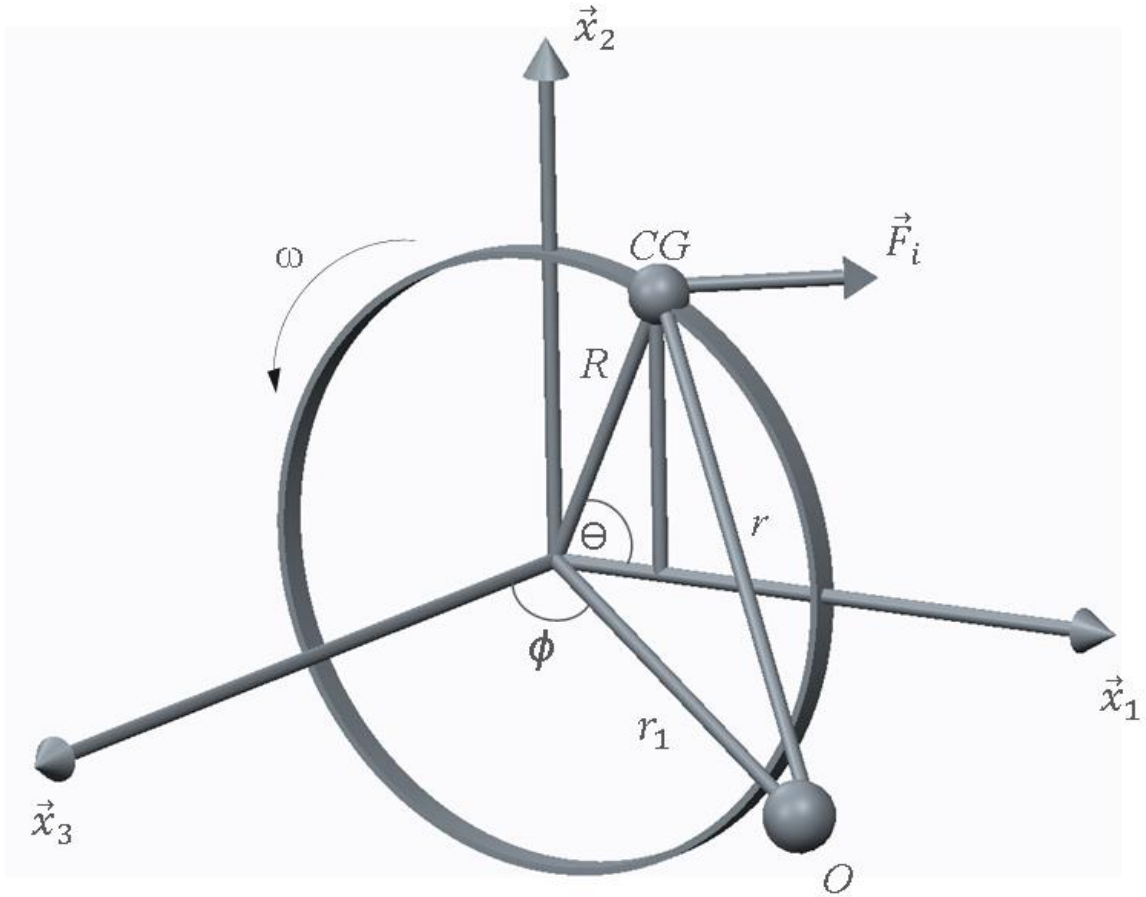
Figure 3: Fan blade acoustic source prediction model coordinate system, Lowson (1970).

The vector force $\vec{F_i}$ is an equivalent point force representing the total distributed force on a compact blade segment, which is calculated using CFD. The point force is then applied at the center of gravity of each blade segment represented by CG in Figure 3. The fan blade segments rotate about $\vec{x_3}$ in the plane defined by $\vec{x_1}$ and $\vec{x_2}$.

It is necessary to determine if the fan blades are acoustically compact or if the fan blades must be split up into smaller acoustically compact segments. According to Howe (2015), an acoustic source is considered acoustically compact if the characteristic size of the source is small compared to the minimum wavelength of interest. The frequency range of interest for the fan considered in this study is 0-1200 Hz. Using 340.29 m/s for the speed

of sound in air, the minimum wavelength of interest 283.6 mm. As shown in Figure 1, the width of each blade is 54.9 mm. This makes the fan blade height 5.2 times smaller than the minimum wavelength of interest. The length of the fan blade is 63.5 mm. This makes the fan blade length 4.5 times smaller than the minimum wavelength of interest. Therefore, the blades are considered acoustically compact and will not need to be split into smaller segments. The SYSNOISE User's Manual (2005) suggests that the characteristic size should be four times smaller than the smallest wavelength of interest making the threshold for acoustic compactness a blade width of 70.8 mm. This makes the size of the acoustic source within the guidelines of the software used.

For the case where the acoustic sources are dipoles representing the forces on the rotating fan blades, Lowson (1970) provides the following solution to equation (2) for the fluctuating sound pressure:

$$p'_{inc\ O,m} = \frac{kmz^2\omega}{2\pi c_0 r_1} \sum_{s=-\infty}^{\infty} (-k)^{mz-s} \left[cos\phi \left(F_3(s) - \left(\frac{mz-s}{mzM}\right) F_1(s) \right) \right] J_{mz-s}(mzMsin\Theta) \tag{3}$$

where $p'_{inc\ O,m}$ is the incident acoustic pressure at the location of the observer O, m is the harmonic number, z is the number of blades, ω is the rotational speed of the blades, r_1 is the distance from the center of rotation to the observer O, c_0 is the speed of sound, M is the rotational Mach number, J is the Bessel function, ϕ is the angle between the axis of rotation $\overrightarrow{x_3}$ and the observer O, k is $\sqrt{-1}$, F_1 is the component of $\overrightarrow{F_i}$ along the $\overrightarrow{x_1}$ axis, F_3 is the component of $\overrightarrow{F_i}$ along the $\overrightarrow{x_3}$ axis, and Θ is the angle between $\overrightarrow{x_1}$ and the center of gravity of the fan blade segment.

13

For the case of the stationary dipole sources acting at the shroud walls, the forces act at the nodes of the acoustic computational mesh as shown in Figure 2. The fluctuating sound pressure induced by a stationary dipoles and solution to equation (2) is:

$$p'_{inc\ O,m} = F_s \frac{\partial G(O|y)}{\partial y_i} \tag{4}$$

where G is the free-field Green's function, F_s is the point force acting at each node, and y_i is the position of each stationary dipole (Russel, 1999).

Once the sound pressure is calculated for the blade and shroud source cases, the overall far field SWL is calculated using the Kirchhoff Formulation detailed by Lyrintzis (2003) for each case individually. The Kirchhoff Formulation calculates the overall far field SWL with a surface integral and sound pressure. The sound pressure from equation (3) for the fan blade source and from equation (4) for the fan shroud source are used with an arbitrary surface outside of the near field that encloses the computational domain.

3.3 EXPERIMENTAL METHOD

Sound power levels where measured in a semi-anechoic chamber to compare with prediction. The experimental setup uses a data acquisition system, pressure microphone array, and power supply to power the fan, as shown in Figure 4.
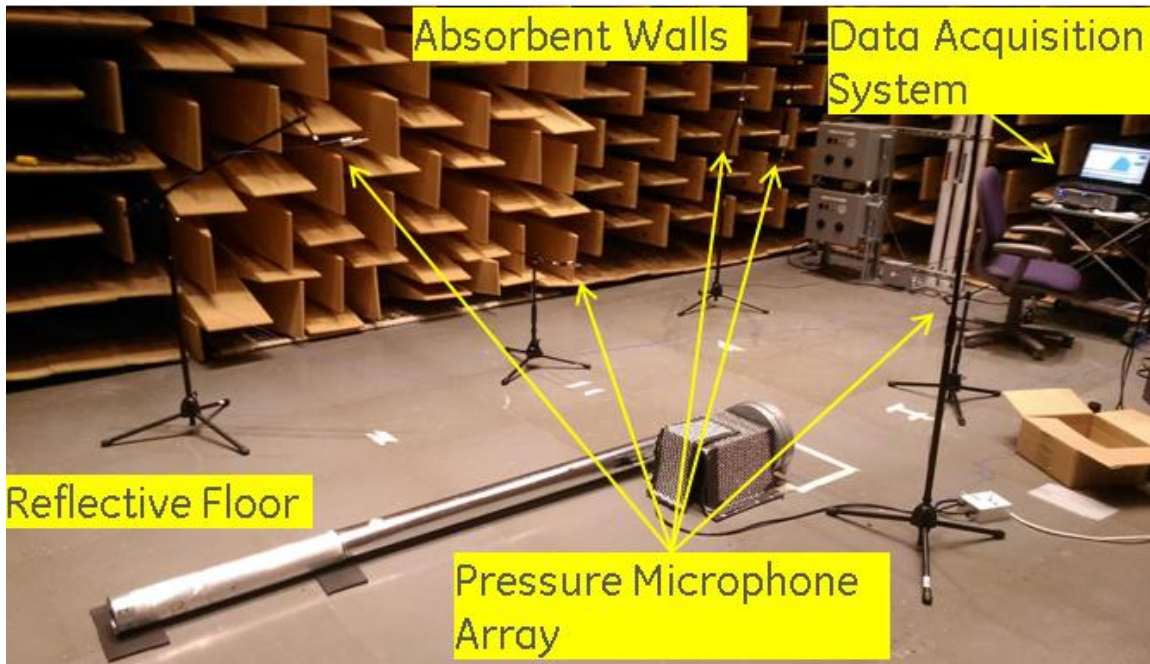
Figure 4: Acoustic measurement instrumentation in semi-anechoic test chamber.

The dimensions of the semi-anechoic chamber are 4.9 m by 6.1 m by 5.8 m. The measured background SWL of the semi-anechoic chamber is 17 dBA. The microphones used were model PCB 378B11 ½" pressure prepolarized microphones from PCB Piezotronics (2014). The manufacturer's accuracy of these microphones is +/-1 dB over a frequency range from 7-7500 Hz. The metal duct shown in Figure 4 extends outside of the control volume defined by the microphones. This locates the outlet restriction outside of the control volume to reduce the amount of outlet restriction noise measured since outlet restriction noise is not being predicted by the acoustic model. Nine microphones were arranged in a grid that defines the measurement surface shown in Figure 5.
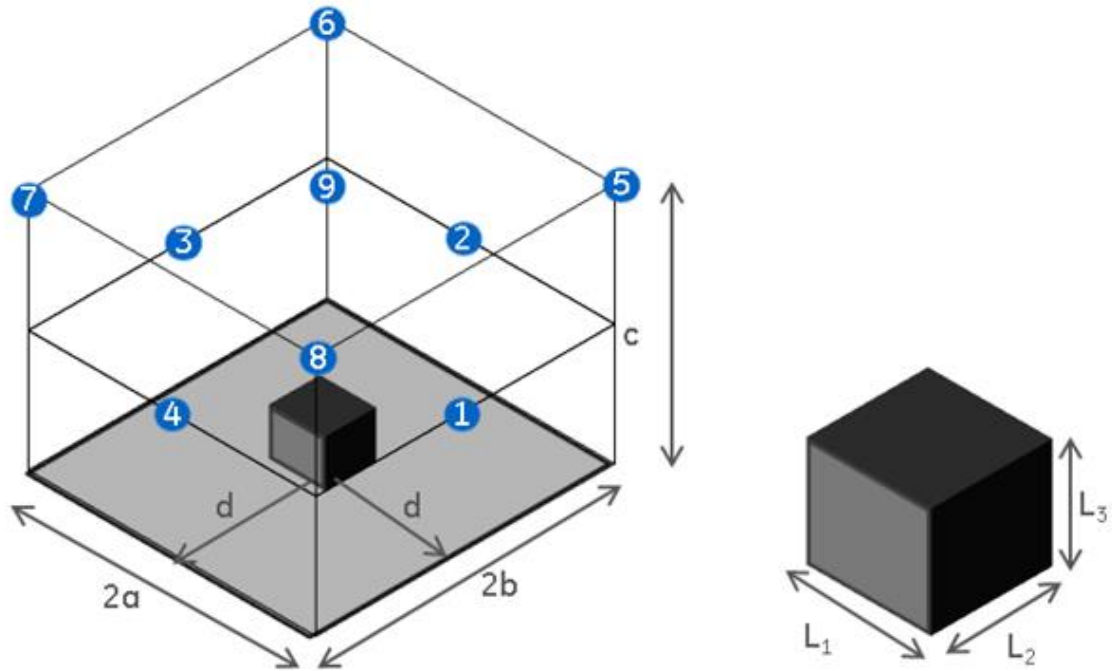
Figure 5: Pressure microphone locations (ISO 7779 (2010)).

The dimensions of the measurement surface and microphone locations are described in ISO 7779 (2010) and are a function of the dimensions of the fan shown in Figure 1. The dimensions of the acoustic source are L_1, L_2 and L_3, where L_1 and L_3 are the diameter of the fan rotor (222 mm) and L_2 is the width of the fan blades (54.9 mm). The dimensions of the measurement surface are sized based on the fan rotor because the fan rotor was considered the primary source of noise. The relationship between the dimensions of the acoustic source and the dimensions of the control volume: a,b, and c in meters are as follows (ISO 7779 (2010)):

$$a = 0.5L_1 + 1 \tag{5}$$

$$b = 0.5L_2 + 1 \tag{6}$$

$$c = L_3 + 1 \tag{7}$$

These dimensions ensure that the microphones are outside of the near field of the acoustic source. Overall far field SWL is calculated from the measured SPL from the following equation:

$$SWL = SPL_{avg} + 10\log\left(\frac{S}{S_0}\right) \tag{8}$$

where S is the total area of the measurement surface taken from the dimensions in Figure 5, S_0 is a reference area of 1 m^2, and SPL_{avg} is the average SPL calculated from the measured SPL of all nine microphones.

The fan was tested at a variety of operating conditions listed in Table 2, where fan speed was measured with a strobe tachometer.

Test Case	RPM	Outlet Restriction Diameter (mm)
1	1778	76.2
2	1482	
3	1778	69.9
4	1564	
5	1778	63.5
6	1606	

Table 2: Fan system operating conditions.

The outlet duct of the fan shroud assembly was restricted with steel plates fixed over the end of the exit duct. The restriction plates are shown in Figure 6.

17
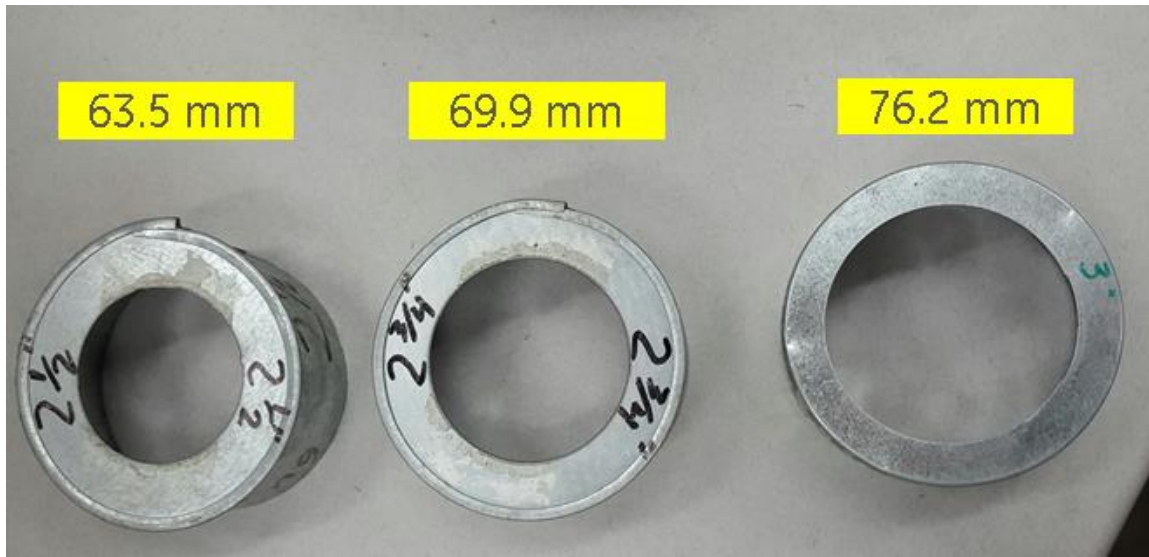
Figure 6: Fan system duct outlet restriction plates.

Three low and three high speed cases were investigated. The high fan speed cases where achieved by operating the fan drive motor at the fan motor's prescribed operating voltage level of 120 volts. The high fan speed cases do not vary between restrictions as the fan motor is operated at its rated voltage. The low fan speed cases were achieved by operating the fan drive motor at one third the fan motor's prescribed operating voltage level. Consequently, the low speed fan cases vary due to the different resistances in flow imparted by the fan outlet restrictions.

4. RESULTS

4.1 AIRFLOW RESULTS

Table 3 compares measured and predicted volumetric flow rates of the fan using the kω-SST turbulence model with a coarse computational mesh at the operating conditions specified for the experiment (Table 2). The level of correlation between predicted and experimentally measured volumetric flow rate is similar to what is achieved by Siwek, Gorski & Fortuna (2014) for the kω-SST turbulence model.

Test Case	RPM	Outlet Restriction Diameter (mm)	Predicted Airflow (m^3/s)	Measured Airflow (m^3/s)	Difference (%)
1	1778	76.2	6.93E-02	7.92E-02	12%
2	1482		5.93E-02	6.53E-02	9%
3	1778	69.9	5.23E-02	6.35E-02	18%
4	1564		4.67E-02	5.77E-02	19%
5	1778	63.5	4.41E-02	4.96E-02	11%
6	1606		4.14E-02	4.66E-02	11%

Table 3: Fan airflow system volumetric flow rate prediction using the kω-SST turbulence model and coarse computational mesh.

As expected, higher fan rotational speeds and larger duct outlet openings resulted in higher flow rates. The calculated fan blade forces and shroud surface forces from these cases are used in the dipole acoustic source models described in section 3.2. In Section 4.2, the effect of the turbulence model and corresponding airflow correlation on the predicted SWL will be discussed.

Results from the kω-SST and SAS turbulence model are provided in Table 4 where predicted versus measured airflow data are compared. For the kω-SST model, the performance for course and fine mesh is also compared. The number of elements in the 'coarse' computational mesh is 4.74E+06. The number of elements in the 'fine' computational mesh is 9.39E+06, or roughly twice as dense as the coarse computational mesh. All computation times shown use 64 computer cores and represent the time to simulate 20 revolutions of the fan.

Turbulence Model	Mesh	Predicted Airflow (m^3/s)	Error (%)	Run Time (hrs)	Increase in run time (%)
kω-SST	Coarse	6.93E-02	12%	52	–
	Fine	6.83E-02	14%	75	44%
SAS		6.73E-02	15%	113	117%

Table 4: Computational mesh size and turbulence model comparison of prediction accuracy and computation time for Test Case 1 (Measured Airflow: 7.92E-02 m^3/s).

Table 4 shows that the finer mesh density does not significantly affect the overall volumetric flow rate prediction and increases the computation time by 44%. The use of the SAS model also does not significantly affect the overall volumetric flow rate prediction and increases the computation time by 117%. Ramakrishna, Krishna, Ramakrishna & Rami (2014) use a similar turbulence model to the SAS model for a shrouded, radial fan and achieved a 15% correlation with measured volumetric flow rate. Therefore, the CFD models used in this paper perform within the level of accuracy of other published data on shrouded, radial, subsonic fans.

4.2 AEROACOUSTIC RESULTS

The overall SWL is calculated using the methods described in section 3.2. Table 5 compares the overall SWL between the measured and predicted results for the kω-SST turbulence model over the operating conditions listed in Table 2. Figure 7 is a graphical representation of the same data.

Test Case	RPM	Outlet Restriction Diameter (mm)	Acoustic Source Model	Predicted SWL (dB)	Measured SWL (dB)	Difference (dB)
1	1778	76.2	Blade	77	79	-2
2	1482			67	73	-6
3	1778	69.9		80	76	4
4	1564			69	75	-6
5	1778	63.5		82	75	7
6	1606			71	72	-1
1	1778	76.2	Shroud	82	79	3
2	1482			70	73	-3
3	1778	69.9		90	76	14
4	1564			85	75	10
5	1778	63.5		79	75	4
6	1606			76	72	4

Table 5: Comparison of the overall far field SWL prediction versus measured for the kω-SST turbulence model with course computational mesh.
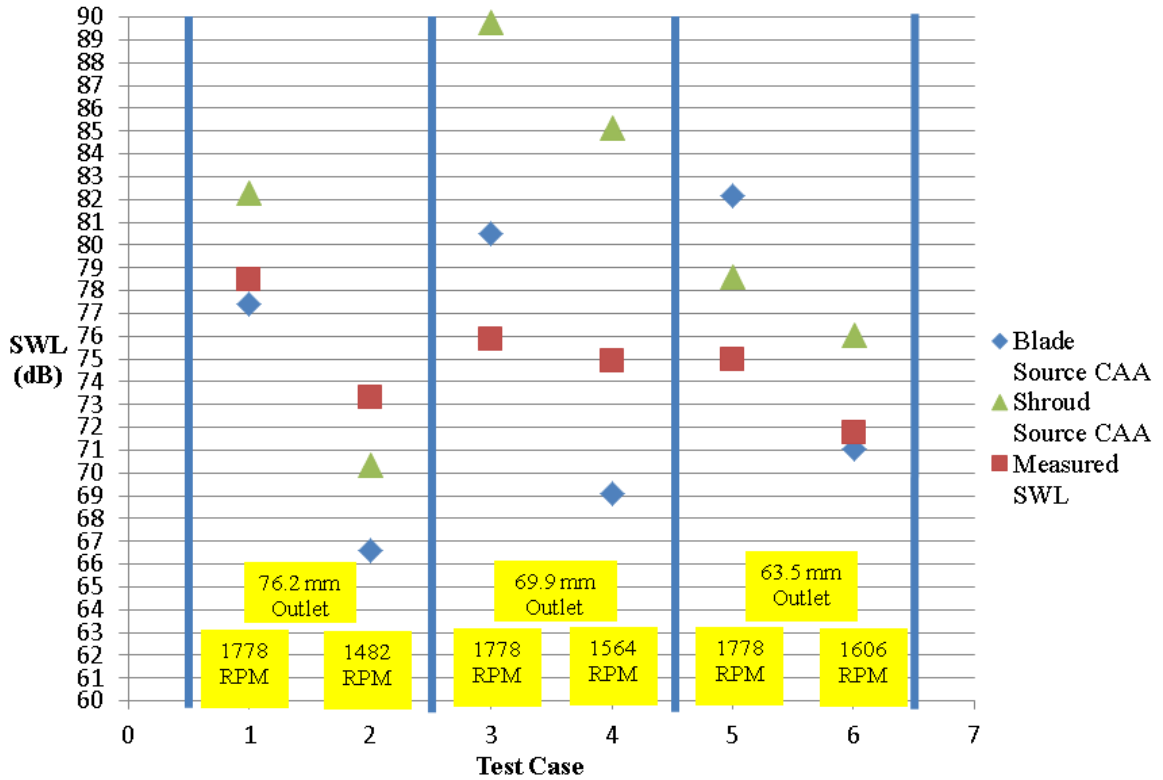
Figure 7: Comparison of the overall far field SWL prediction versus measured for the kω-SST turbulence model with course computational mesh.

The experimental data show an increasing trend between fan rotational speed and overall far field SWL. This is to be expected as the effects of an increase in rotational speed are well understood in one of the fan scaling laws of acoustics summarized by Cory (2005). The acoustic scaling law is given as:

$$SWL_2 = SWL_1 + 55 \frac{logN_2}{logN_1} \qquad (9)$$

where N_1 and N_2 are the rotational speeds of the fan blades in revolutions per minute (RPM). The quantity SWL_1 is the sound power level of the fan at N_1 and SWL_2 is the predicted sound power level of the fan at N_2. Equation (9) shows that given a known overall far field SWL at a known rotational speed, the overall far field SWL at another

rotational speed of the same fan can be predicted. Table 7 shows how the acoustic scaling law calculation compares to the actual test data.

Outlet Restriction Diameter (mm)	Low RPM	High RPM	Low Speed Measured SWL (dB)	High Speed Measured SWL (dB)	Predicted High Speed SWL from Acoustic Scaling Law
76.2	1482		73	79	78
69.9	1564	1778	75	76	78
63.5	1606		72	75	74

Table 6: Acoustic scaling law prediction.

Table 6 shows that the increase in overall measured far field SWL is in agreement with the established fan acoustic scaling laws.

For test cases 1, 2, 5, and 6, the blade source model and shroud source model agree within 5 dBA. For test cases 3 and 4, the discrepancy between the two models is 10 and 16 dBA respectively with the blade source model predicting within 6 dB and the shroud source model predicting within 14 dBA of overall measured far field SWL. Table 3 shows there is a greater discrepancy between the measured and predicted volumetric flow rate for test cases 3 and 4 than the other four test cases. It is possible that the fluid flow around the fan shroud is not being adequately resolved by the CFD model for test cases 3 and 4 and this is causing significant error in the overall shroud source model SWL prediction for these cases.

For Test Case 1, a computational mesh coarseness and turbulence model study was performed to determine their influence on predicting overall far field SWL. Since the blade source model has been shown to be more accurate in general, it is used here. The CFD data from the modeling conditions listed in Table 4 are used as acoustic sources.

Table 7 shows the overall far field SWL prediction comparison between turbulence models and computational mesh density used.

Mesh	Turbulence	Predicted SWL (dB)	Measured SWL (dB)	Difference (dB)
Coarse	kω-SST	77		-2
Fine	kω-SST	79	79	0
Fine	SAS	80		1

Table 7: Test Case 1 blade source turbulence model overall far field SWL comparison.

The overall far field SWL prediction is not significantly improved by computational mesh density or turbulence model. Ramakrishna, Krishna, Ramakrishna & Rami (2014) used a similar turbulence model to SAS and calculated on average an 8 dB difference between predicted and measured SPL. Therefore the overall far field SWL prediction is within expectations for an acoustic source generated using SAS.
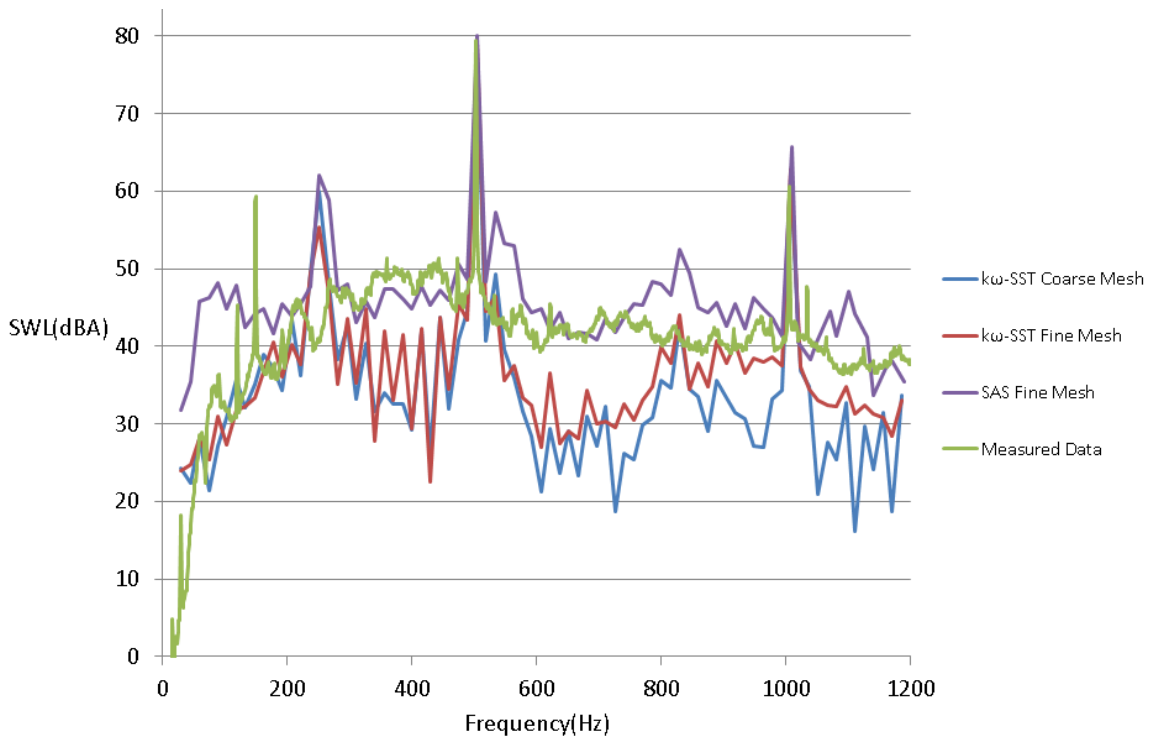

Figure 8: Broadband spectrum comparison between the different turbulence models and the measured spectrum.

Figure 8 shows a broadband spectrum comparison between the different turbulence models and the measured spectrum. The SAS turbulence model predicts the broadband spectrum more accurately than the kω-SST model with both coarse and fine computational meshes. However, as shown in table 7, broadband spectrum accuracy does not improve the overall far field SWL prediction since, for the shrouded fan considered in this study, tonal noise dominates. Table 4 shows the advantage of using a less dense computational mesh or less computationally intensive turbulence model. If the acoustic response of the fan being analyzed is known to be tonal, then using the kω-SST turbulence model with a coarse computational mesh is shown here to be adequate.

4.3 COMPARISON TO LITERATURE

Younsi, Bakir & Kouidri (2008) performed a similar study on a shrouded, radial fan. They used the kω-SST turbulence model in their CFD solution, the time varying forces on the impeller blades as an acoustic source and calculated the acoustic response using the FW-H acoustic analogy. Younsi et al. (2008) measured SPL using a single microphone in a semi-anechoic chamber. Table 8 shows the prediction comparison of several different blade designs. Model VA160 has 39 fan blades spaced evenly on a 160 mm diameter impeller. Model VA160D is the same as VA160 but has irregular blade spacing. VA150 has an impeller diameter of 150 mm but in all other respects is the same as VA160. VA160E has 19 regularly spaced blades and has a hub diameter of 160 mm. The values of Table 8 are shown in Figure 9 in graphical form.

25

Test Case	Design	RPM	CAA SPL	Test SPL	dB Difference
1	VA160	3000	51	57	-6
2	VA160D	3000	47	57	-10
3	VA150	3200	45	53	-8
4	VA160E	2900	64	78	-14

Table 8: Overall SPL prediction comparison using the kω-SST turbulence model (Younsi et al. 2008)
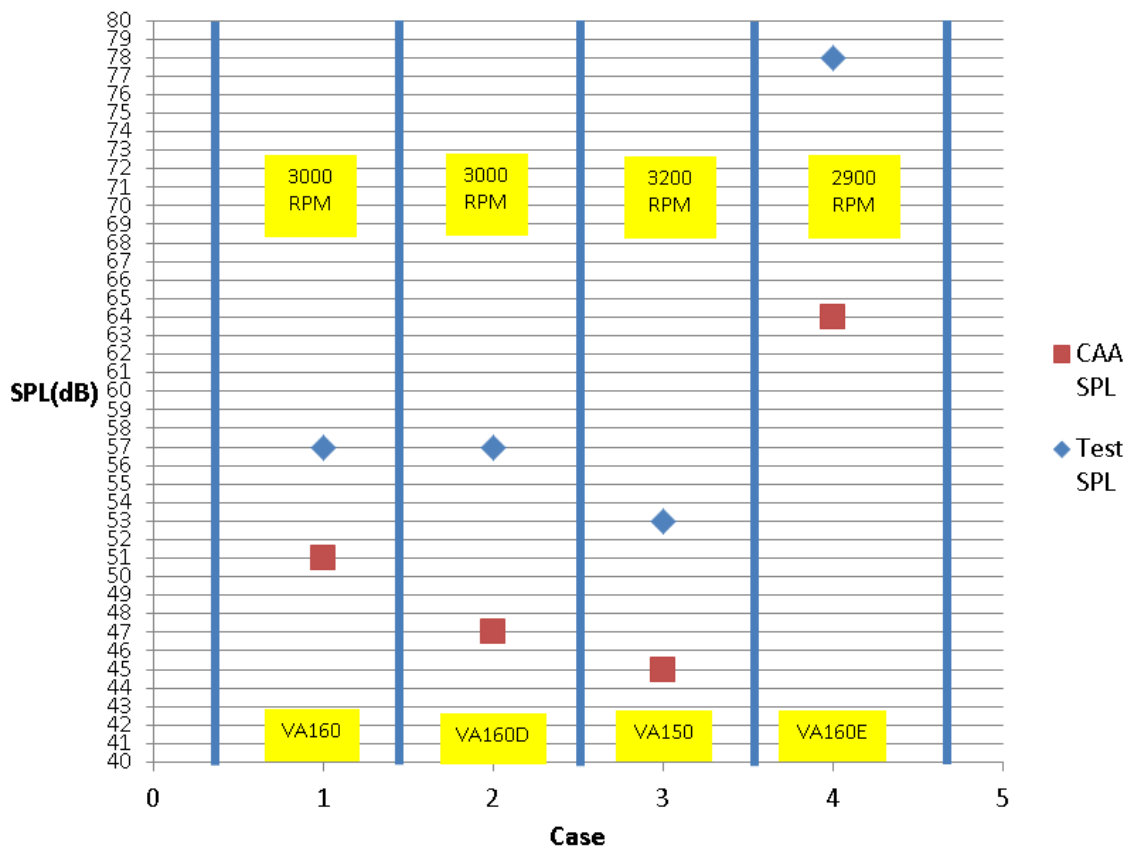

Figure 9: Overall SPL prediction comparison (Younsi et al. 2008)

The overall blade source SPL prediction by Younsi et al. (2008) differs from measured data by 6 to 14 dB. The current study blade source overall far field SWL prediction differs from 1 to 7 dB. Both studies are using the same kω-SST turbulence model on a similar fan, but is not accounting for the diffraction, focusing and scattering effects of the

26

fan shroud as a part of the aeroacoustic simulation. Younsi et al. (2008) are also predicting SPL at a single microphone location. It is possible that the acoustic model is consistently under predicting SPL because the fan shroud is changing the directionality to the radiated sound and the test microphone is in an area with higher SPL as a result.

Figure 10 shows a broadband spectrum comparison between the measured data and the prediction.
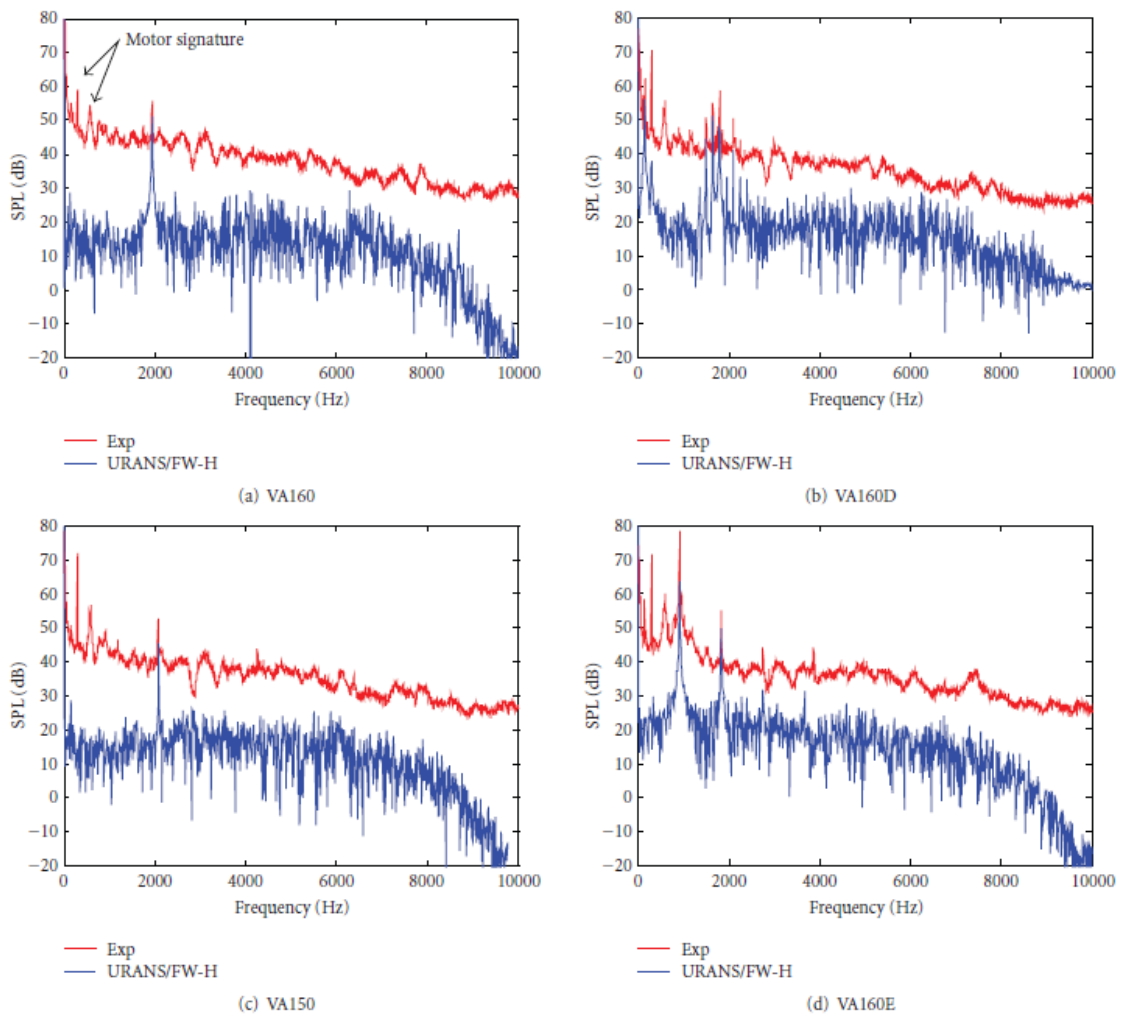

Figure 10: Broadband spectrum SPL comparison Younsi et al. (2008)

In Figure 10, the URANS/FW-H represents the predicted data and Exp represents the measured data. A much larger frequency range is calculated by Younsi et al. (2008) than what is calculated in the current study. Figure 10 shows that Younsi et al. (2008) had less success than the current study at predicting broadband noise content using the kω-SST turbulence model. Broadband predictions differ from measurement by an average of 20 dB for Younsi et al. (2008) and off by 10 dBA in the current study. The larger discrepancy shown by Younsi et al. (2008) is possibly due to the same modeling and testing techniques that explain the discrepancy in predicted overall SPL. The effect of the fan shroud on the directionality of the radiated sound could account for the consistent under prediction of the broadband noise content at the single microphone location.

5. SUMMARY/CONCLUSIONS

The overall far field SWL prediction using the kω-SST turbulence model agreed reasonably well with the measured results. Modeling the acoustic source of a shrouded, radial fan as rotating dipoles located at the center of gravity of each fan blade, or blade model, was shown to be more accurate in general at predicting sound power level than modeling the source as a field of distributed stationary dipoles located on the interior surface of the fan shroud, or shroud model. The discrepancies between measured and predicted overall far field SWL ranged from 1 dBA to 7 dBA difference for the blade model and 3 dBA to 14 dBA difference for the shroud model. Agreement between predicted and measured airflow is shown to have an influence on overall far field SWL predication for the shroud source model.

Younsi, Bakir & Kouidri (2008) performed a similar study to the blade model and experienced a range of 3 dB to 14 dB difference between prediction and measured SPL over a range of fan designs using a blade source model. The current study accounts for the fan shroud in the acoustic prediction model where Younsi et al. did not and this possibly explains the increased accuracy.

The SAS model increases the computation time by 117% over the kω-SST model with only a 1 dBA improvement in overall far field SWL prediction. The SAS model does, however, increase the broadband noise prediction accuracy by 10 dBA over frequencies ranging from 600 to 1000 Hz. The overall far field SWL of the shrouded, radial, subsonic

fan in this study is dominated by tonal noise characteristics, so the improvement in broadband noise prediction is not seen in the overall far field SWL.

6. FUTURE WORK

There are several areas that are worth investigating in order to improve the acoustic prediction for a radial, shrouded fan. The SAS turbulence model for this study was only used at one operating point. At this operating point, the broadband prediction significantly improved over the kω-SST turbulence model, but the overall far field SWL did not significantly improve. This was possibly due to the overall far field SWL being dominated by tonal characteristics. A study of fan with mostly broadband characteristics would be beneficial to investigate the improved accuracy possible with the SAS model.

Acoustic compactness of the fan blades is one area that should receive attention for study. Based on guidelines suggested by the developer of the CAA software used, the blades did not need to be split into smaller segments and were acoustically compact. However, this assumption could be validated or refuted with a blade segmentation sensitivity study.

The monopole and quadrupole acoustic source terms from the FW-H aeroacoustic analogy were ignored for the purposes of this paper based recommendations from previous works. Both the monopole and quadrupole source terms should be investigated for this fan in order to quantify the effect of volumetric flow rate and turbulent stresses in the flow on the overall acoustic prediction.

REFERENCES

ANSYS Fluent (2015). ANSYS Fluent Theory Guide. Retrieved February 2, 2015 from https://support.ansys.com/AnsysCustomerPortal/en_us/Knowledge+Resources/Online+Documentation/Current+Release

Colonius, T., & Lele, S. (2004). Computational aeroacoustics: progress on nonlinear problems of sound generation. *Progress In Aerospace Sciences*, *40*(6), 345-416. Doi:10.1016/j.paerosci.2004.09.001

Cory, W. (2005). *Fans & ventilation*. Amsterdam: Elsevier in association with Roles & Assoc.

Curle, N. (1955). The Influence of Solid Boundaries upon Aerodynamic Sound. *Proceedings Of The Royal Society A: Mathematical, Physical And Engineering Sciences*, *231*(1187), 505-514. Doi:10.1098/rspa.1955.0191

Date, A. (2005). *Introduction to computational fluid dynamics*. New York: Cambridge University Press.

Eymard, R., Gallouet, T., & Herbin, R. (1997). Finite Volume Methods. In P. Ciarlet & J. Lions, *Handbook of Numerical Analysis* (1st ed., pp. 713-1020). Marseille: LATP, UMR 6632.

Howe, M. (2015). *Acoustics and aerodynamic sound*. Cambridge: Cambridge University Press.

Huang, P. G., Bardina, J. E., & Coakley, T. J. (1997). Turbulence Modeling Validation, Testing, and Development. *NASA Technical Memorandum*, *110446*.

HYPERMESH rev.8.0, User's Guide, Altair Engineering Inc., Troy, MI (2006).

ISO, (2010). ISO 7779:2010 − Acoustics − Measurement of airborne noise emitted by information technology and telecommunications equipment.

Jeon, W., Baek, S., & Kim, C. (2003). Analysis of the aeroacoustic characteristics of the centrifugal fan in a vacuum cleaner. *Journal Of Sound And Vibration*, *268*(5), 1025-1035. Doi:10.1016/s0022-460x(03)00319-5

Lighthill, M. (1954). On Sound Generated Aerodynamically. II. Turbulence as a Source of Sound. *Proceedings Of The Royal Society A: Mathematical, Physical And Engineering Sciences*, *222*(1148), 1-32. Doi:10.1098/rspa.1954.0049

Lighthill, M. (1952). On Sound Generated Aerodynamically. I. General Theory. *Proceedings Of The Royal Society A: Mathematical, Physical And Engineering Sciences*, *211*(1107), 564-587. Doi:10.1098/rspa.1952.0060

Lowson, M. (1970). Theoretical Analysis of Compressor Noise. *The Journal Of The Acoustical Society Of America*, *47*(1B), 371. doi:10.1121/1.1911508

Lyrintzis, A. (2003). Surface integral methods in computational aeroacoustics—From the (CFD) near-field to the (Acoustic) far-field. *International Journal Of Aeroacoustics*, *2*(2), 95-128. Doi:10.1260/147547203322775498

Mendonça, F., Allen, R., De Charentenay, J., & Lewis, M. (2002, October). Towards understanding LES and DES for industrial aeroacoustic predictions. In *Int. Workshop on LES for Acoustics, DLR Göttingen, Germany, 7–8 October 2002*.

Menter, F. R., Kuntz, M., & Langtry, R. (2003). Ten years of industrial experience with the SST turbulence model. *Turbulence, Heat and Mass Transfer 4*.

Menter, F., & Egorov, Y. (2005). A Scale-Adaptive Simulation Model using Two-Equation Models. In *AIAA Aerospace Sciences Meeting and Exhibit*. Reno, Nevada.

Pradera, A., Rivas, A., Gil-Negrete, N., Vinolas, J., & Schram, C. (2005). Numerical Prediction of the Aerodynamic Noise Radiated by a Centrifugal Fan. In *Twelfth International Congress on Sound and Vibration*. Lisbon, Portugal.

PCB Piezotronics, Installation and Operating Manual, PCB Group, Depew, New York, (2014).

Ramakrishna, S., Krishna, V., Ramakrishna, A., & Ramji, K. (2014). CFD and CAA Analysis of Centrifugal Fan for Noise Reduction. *International Journal Of Computer Applications*, *86*(7), 10-16. doi:10.5120/14996-3008

Russell, D. (1999). Acoustic monopoles, dipoles, and quadrupoles: An experiment revisited. *Am. J. Phys., 67*(8), 660. doi:10.1119/1.19349

Siwek, T., Gorski, J., & Fortuna, S. (2014). Numerical and Experimental Study of Centrifugal Fan Flow Structures and Their Relationship with Machine Efficiency. *Polish Journal Of Environmental Studies*, *23*(6), 2359-2364.

Sorguven, E., Dogan, Y., Bayraktar, F., & Sanliturk, K. (2009). Noise prediction via large eddy simulation: Application to radial fans. *Noise Control Eng. J.*, *57*(3), 169. doi:10.3397/1.3117158

SYSNOISE rev.5.6, User'sManual, LMS Numerical Technologies, Leuven, Belgium, (2005).

Tournour, M., EL Hachemi, Z., Read, A., Mendonca, F., Barone, F., & Durello, P. (2003). Investigation of the Tonal Noise Radiated by Subsonic Fans Using the Aero-Acoustic Analogy. In *FAN NOISE 2003* (pp. 1-8). Senlis: International Symposium Senlis.

Williams, J., & Hawkings, D. (1969). Sound Generation by Turbulence and Surfaces in Arbitrary Motion. *Philosophical Transactions Of The Royal Society A: Mathematical, Physical And Engineering Sciences*, *264*(1151), 321-342. Doi:10.1098/rsta.1969.0031

Younsi, M., Bakir, F., Kouidri, S., & Rey, R. (2006, January). 2D and 3D unsteady flow in squirrel-cage centrifugal fan and aeroacoustic behavior. In *ASME 2006 2nd Joint US-European Fluids Engineering Summer Meeting Collocated With the 14th International Conference on Nuclear Engineering* (pp. 805-813). American Society of Mechanical Engineers.

Younsi, M., Bakir, F., Kouidri, S., & Rey, R. (2007). Numerical and experimental study of unsteady flow in a centrifugal fan. *Proceedings of the Institution of Mechanical Engineers, Part A: Journal of Power and Energy*, *221*(7), 1025-1036.

Younsi, M., Bakir, F., Kouidri, S., & Rey, R. (2008). Influence of impeller geometry on the unsteady flow in a centrifugal fan: numerical and experimental analyses. *International Journal of Rotating Machinery*, *2007*.

APPENDICES

Appendix A: Computational Fluid Dynamics Computational Mesh

Appendix B: Computational Aeroacoustics Computational Mesh

Appendix C: Airflow Test Setup

Appendix D: CFD Boundary Conditions

Appendix E: CFD Convergence Behavior

Appendix A: Computational Fluid Dynamics Computational Mesh

A computational mesh was constructed to represent the fluid domain of the computational fluid dynamics model. An inlet region was generated to represent the air in the room entering the fan shroud inlet and is shown in detail in Figure 11.
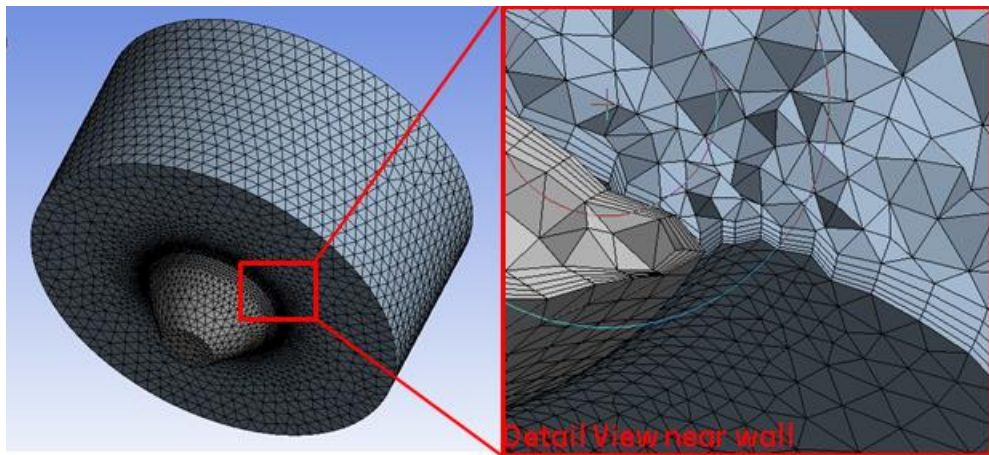
Figure 11: Inlet region mesh and detailed view.

An inflation layer is required near the walls to adequately resolve the wall boundary layer. The stationary housing region is shown in Figure 12. A similar inflation layer is required in this region of the mesh.
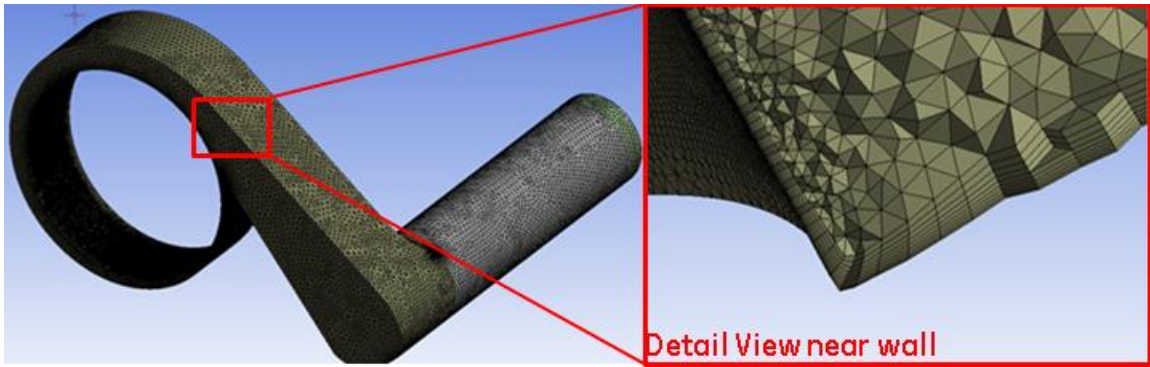
Figure 12: Shroud region mesh and detailed view.

The stationary inlet and housing meshes were generating using the ANSYS Fluent (2015) meshing tool.

The rotating blade region was generated using ANSYS Turbogrid (2015) meshing tool. This software spatially discretizes the domain into hexahedral elements with the best quality possible. Figure 13 shows how the blade region was discretized.
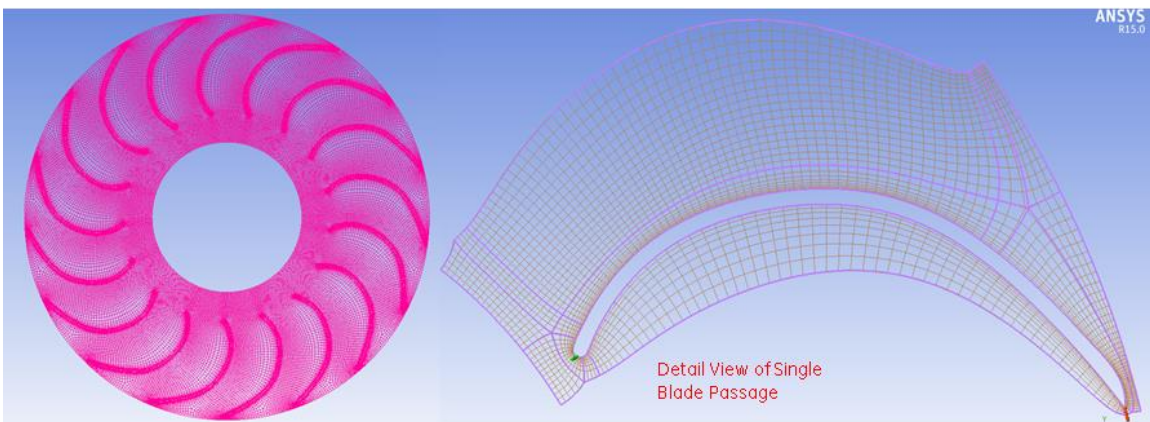

Figure 13: Rotating bade region mesh and detailed view

Appendix B: Computational Aeroacoustics Computational Mesh

The finite element acoustic mesh was generated using HYPERMESH (2006). The mesh elements are tetrahedrons with the maximum edge length set to one sixth of the minimum wavelength of interest as per the SYSNOISE (2005) guidelines.
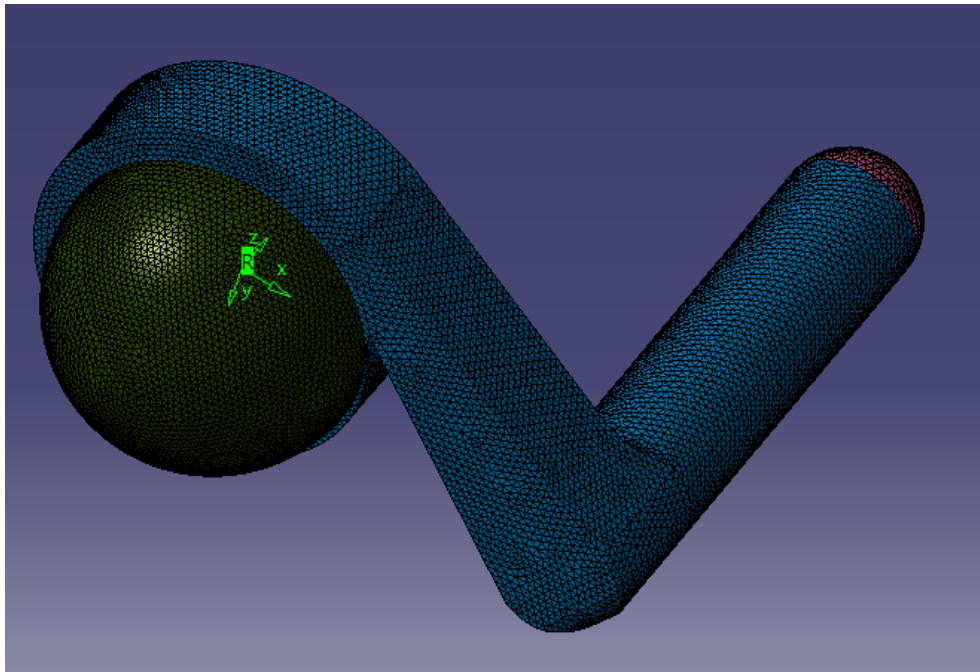

Figure 14: Finite element aeroacoustic mesh.

Appendix C: Airflow Test Setup

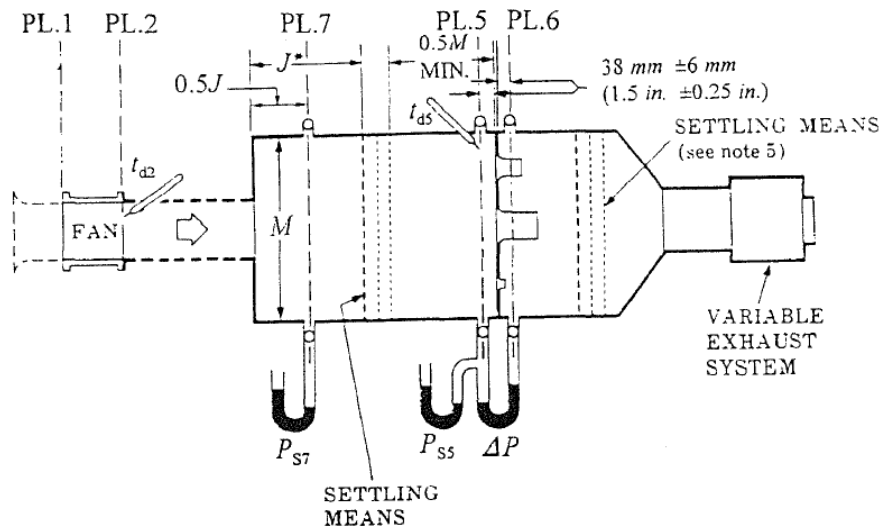Figure 15 shows the diagram provided by the AMCA 210 standard for airflow test chamber measurements.

Figure 15: Air flow chamber (AMCA 210 31)

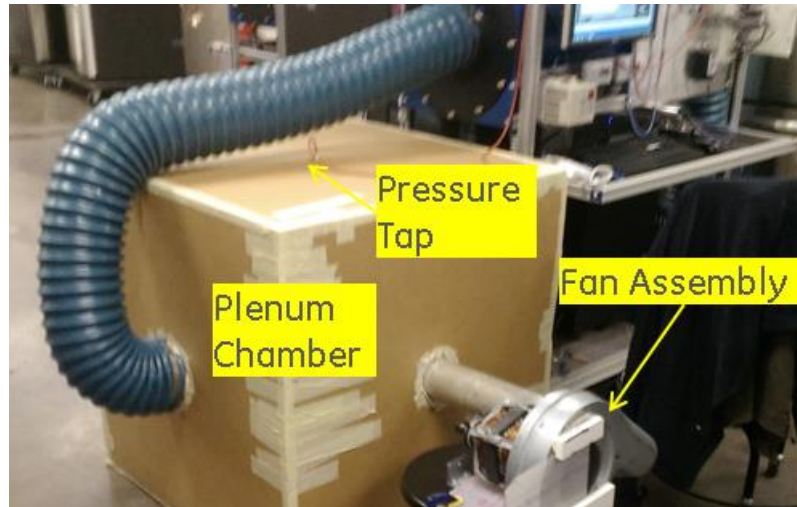Figures 16 and 17 show a detailed view of the devices used in the airflow test setup.
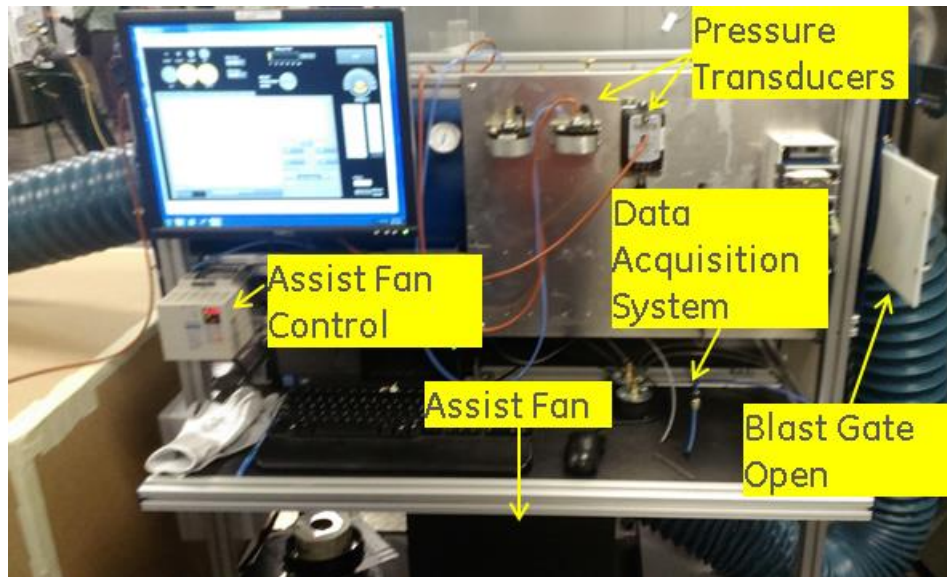
Figure 16: Airflow measurement system part 1

Figure 17: Airflow measurement system part 2

Appendix D: CFD Boundary Conditions

The boundary conditions for the CFD model are atmospheric inlet and outlet pressure and a constant rotational speed applied to the region of air surrounding the fan blades. Figure 18 shows the location of the boundary conditions. The airflow restrictions from Figure 6 are modeled as a porous media. Porous media condition was used to represent the airflow restriction to use the same computational mesh to model different restructions.
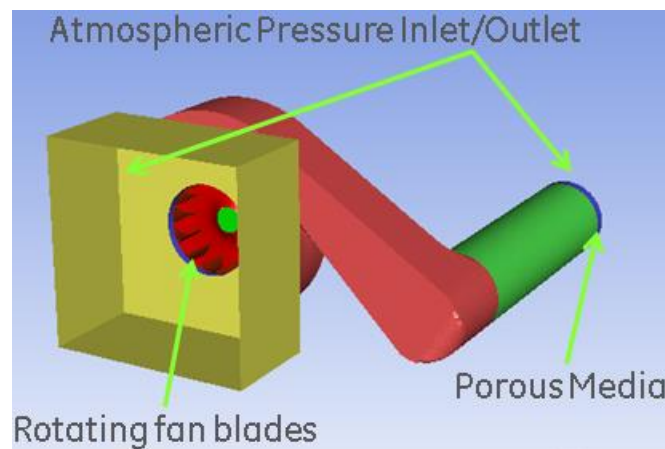

Figure 18: Computational Fluid dynamics boundary conditions part 1

Figure 19 shows the regions of stationary and rotating mesh. The area around the fan blades rotates at a constant speed.
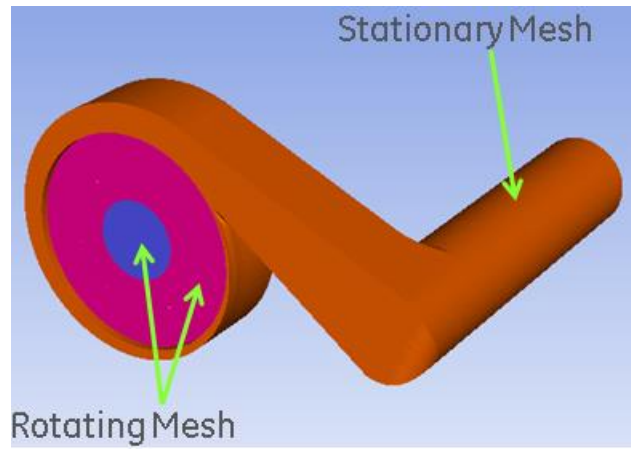
Figure 19: Computational Fluid Dynamics boundary conditions part 2

Appendix E: CFD Convergence Behavior

Figure 20 shows the computed airflow and pressure data for test case 1 using the kω-SST turbulence model and coarse mesh. This represents typical convergence behavior for the other 5 test cases. The model converges to a steady state solution after five complete revolutions of the fan rotor. The simulation is executed for five additional revolutions to ensure that the model has converged and is stable. The acoustic prediction requires ten revolutions of converged aerodynamic data so the simulation is executed for another ten revolutions. This results in a total of twenty simulated revolutions.
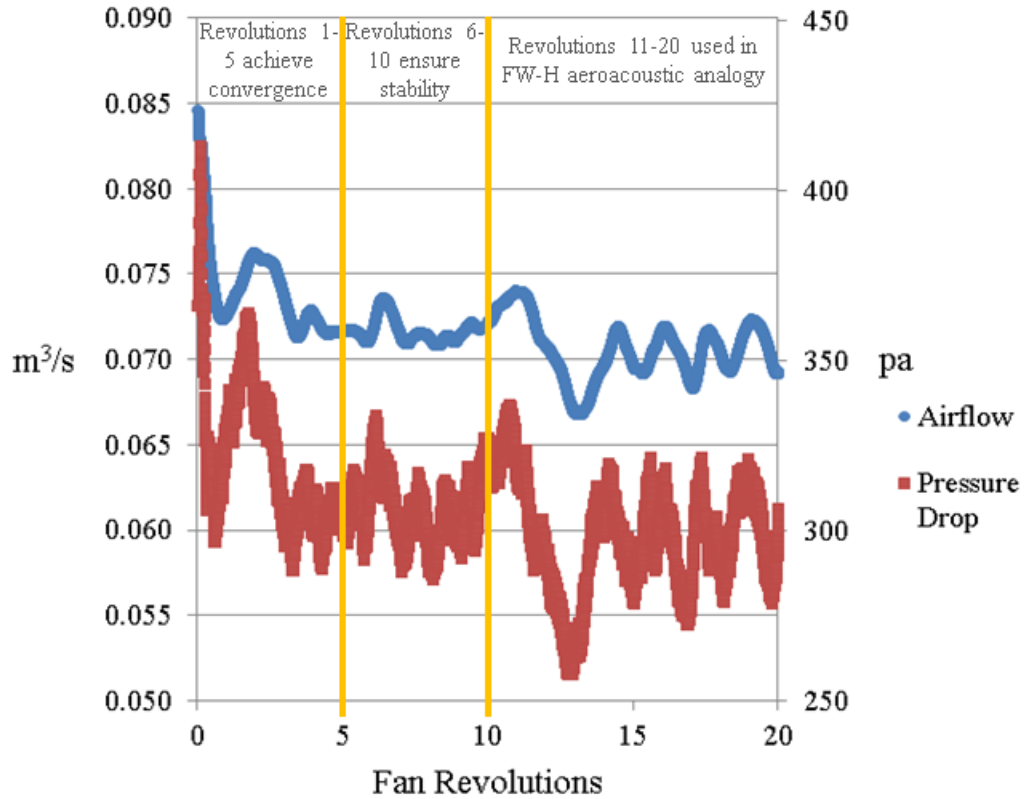
Figure 20: Airflow computational model convergence for kω-SST model with a coarse computational mesh (Test Case 1).

There is a computational disturbance after ten revolutions. This is an artifact of the computation fluid dynamics software and is not a response to any change in the model. The average volumetric flow rate and pressure drop across the fan have not changed significantly after this event, so the solution is still considered converged.

CURRICULUM VITA

NAME: Bryan Buccieri

CONTACT: armads6@yahoo.com
Work: 502-452-4555
Cell: 502-457-6946
5505 Overbrook Woods Place
Unit 204
Louisville, KY 40291

DOB: March 21, 1990

EDUCATION
& TRAINING: M.S. Mechanical Engineering (exp. 12/2015)
University of Louisville
(GPA: 3.84/4.0)
2012-Present

B.S. Mechanical Engineering
Rose-Hulman Institute of Technology
(GPA: 3.2/4.0)
2008-2012

WORK EXPERIENCE:

GE Appliances, Louisville, KY   July 2012-2015
Edison Engineering Development Program

5th Rotation, CAE: Predictive Models/ CFD   July 2014-Present

- Gained competency in CFD numerical modeling.
- Modeled fluids and acoustics

4th Rotation, Refrigeration: NPI   January 2014-Jul 2014

- Planned and executed test plan to qualify thermal and energy performance of bottom freezer refrigerators

3ʳᵈ Rotation, Laundry: Platform   July 2013-Jananuary 2014

- Validation of numerical stress model with strain gauge testing of steel wash baskets
- Analyzed field data to develop and developed wash cycle to reduce occurrence of tangling

2ⁿᵈ Rotation, HEWH: Platform   January 2013-July 2013

- Designed and executed test plan to quantify test error induced by variation to test procedure in energy testing
- Quantified systemic error in energy testing

1ˢᵗ Rotation, Refrigeration: NPI   July 2012-January 2013

- Qualified production fixtures for door foam process
- Developed long term door alignment control data

LABORATORY TECHNIQUES:

Fan/ System curve set-up, Semi Anechoic chamber, and design of experiments

COMPUTER SKILLS/ LANGUAGES:

Knowledgeable: SolidWorks, ANSYS Workbench, ANSYS Fluent, MiniTab, Microsoft Word, Excel, PowerPoint

Basic Understanding: MATLAB, LabVIEW